Physics opportunities for a fixed-target programme in the ALICE experiment

F. Galluccio[a], C. Hadjidakis[b], D. Kikoła[c], A. Kurepin[d], L. Massacrier[b,*], S. Porteboeuf[e], K. Pressard[b], W. Scandale[f], N. Topilskaya[d], B. Trzeciak[g], A. Uras[h]

[a]*INFN, Sezione di Napoli, Complesso Universitario di Monte Sant'Angelo, Via Cintia, 80126 Naples, Italy*
[b]*IPNO, CNRS-IN2P3, Univ. Paris-Sud, Université Paris-Saclay, 91406 Orsay Cedex, France*
[c]*Faculty of Physics, Warsaw University of Technology, ul. Koszykowa 75, 00-662 Warsaw, Poland*
[d]*Institute for Nuclear Research, Moscow, Russia*
[e]*Université Clermont Auvergne, CNRS/IN2P3, LPC, F-63000 Clermont-Ferrand, France.*
[f]*CERN, European Organization for Nuclear Research, 1211 Geneva 23, Switzerland*
[g]*Institute for Subatomic Physics, Utrecht University, Utrecht, The Netherlands*
[h]*IPNL, Université Claude Bernard Lyon-I and CNRS-IN2P3, Villeurbanne, France*

Abstract

A fixed-target programme in the ALICE experiment using the LHC proton and lead beams offers many physics opportunities related to the parton content of the nucleon and nucleus at high-x, the nucleon spin and the Quark-Gluon Plasma. We investigate two solutions that would allow ALICE to run in a fixed-target mode: the internal solid target coupled to a bent crystal and the internal gas target. The feasibility of these solutions are being studied for a possible installation at the LHC interaction point IP2 during the Long Shutdown 3.

*Corresponding author. Email: laure.marie.massacrier@cern.ch

1. Executive summary

Physics motivation. The physics opportunities offered by a fixed target programme at the LHC have been developed in several publications of the AFTER@LHC study group [1, 2, 3, 4]. These cover studies of the large-x gluon, sea quark and heavy-quark content in the nucleon and nucleus and its connection to astroparticles, the dynamics and spin of gluons inside polarised nucleons (if a polarised target were used), and the Quark-Gluon Plasma formed in heavy-ion collisions between SPS and RHIC energies. The central barrel and muon detectors of the ALICE experiment, running in a fixed-target mode, will provide access to two rapidity ranges: the far backward centre-of-mass rapidity range for the central barrel and the backward to mid centre-of-mass rapidity range for the muon spectrometer. Heavy-flavor and Drell-Yan production will allow one to probe the high-x content of the nucleon and nuclei in pp and pA collisions. In PbA collisons, identified charged particles as well as heavy-flavor production will provide constraints on the properties of the Quark-Gluon Plasma towards large rapidities. In the central barrel, antiproton measurements will bring new inputs to astroparticle physics. Finally, a polarised target will open the possibilities to probe the spin content of the nucleon towards high-x for various probes.

Implementation. Two solutions are being investigated to deliver fixed-target collisions in ALICE: an internal solid target coupled to a bent crystal installed prior of the LHC Interaction Point 2 (IP2) that deviates the beam halo, and a gas target. These solutions provide large luminosities in pp, pA and PbA collisions.

Estimated performance and timescale. In the bent crystal case, fluxes of 5×10^8 s^{-1} and 10^5 s^{-1} for the proton and lead beams are considered. For the gas target, an areal density up to 10^{31} atoms/cm^2 for H_2 can be expected. A parallel running with ALICE operating in colliding mode is envisioned. A dedicated running time could possibly be planned, in particular with the proton beam. If no showstoppers are identified, the implementation could take place during the LHC Long Shutdown 3 in order to take data in LHC Run 4.

Challenges. Studies are ongoing to assess the challenges of this proposal. On one hand, the LHC machine protection and the compatibility of the fixed-target operation at IP2 with the collimation and vacuum operation need to be evaluated from the accelerator complex side. On the other hand, the target system integration in the ALICE experiment as well as the ALICE detector performances in a fixed-target mode need to be studied. Some of these studies will be carried out within the Horizon 2020 grant *STRONG-2020*.

2. Introduction

Fixed-target experiments present many advantages having the versatility of polarised and nuclear targets and allowing to reach high luminosities with dense and long targets. The LHC 7 TeV proton and 2.76 A TeV lead beams on a fixed-target allow one to reach a center-of-mass energy per nucleon pair of $\sqrt{s_{\rm NN}} = 115$ GeV and $\sqrt{s_{\rm NN}} = 72$ GeV with a center-of-mass rapidity boost of 4.8 and 4.2 units, respectively. These energies correspond to an energy domain between SPS and nominal RHIC energies. The large rapidity boost implies that the backward rapidity region ($y_{cms} \leq 0$) is easily accessible by using standard experimental techniques. The ALICE detectors provide many physics opportunities if running in fixed-target mode with the LHC proton and lead beams. One of the main strength of ALICE is its large rapidity coverage. Assuming a target location at $z = 0$, the ALICE Muon Spectrometer (MS) gives access to the mid- to backward rapidity in the center-of-mass frame ($-2.3 < y_{\rm cms} < -0.8$)[1]. In addition, the absorber in front of the muon tracking station is an asset for background rejection and Drell-Yan studies, that probe the sea quark content of the nucleon and nucleus. The ALICE Central Barrel (CB) offers a complementary coverage to the muon arm by accessing the very backward rapidity region ($-5.7 < y_{\rm cms} < -3.9$), reaching the end of phase space for several probes. Thanks to its particle detection and identification capabilities, down to low $p_{\rm T}$, unique measurement of soft probes

[1] considering an incident proton beam on the target. For an incident lead beam, the ALICE MS rapidity coverage is $-1.8 < y_{\rm cms} < -0.3$ and ALICE CB coverage $-5.2 < y_{\rm cms} < -3.4$. Massless particles are assumed to compute the rapidity coverage.

and open heavy flavours can be pursued. Another asset of the ALICE apparatus is the capability to operate with good performances in a high particle density environment. Access to most central AA collisions at $\sqrt{s_{NN}} = 72$ GeV should be possible if the interaction rate remains low. In addition, the ALICE Collaboration could potentially devote a significant data taking time to a fixed-target programme (especially with the proton beam), allowing the collection of large integrated luminosities and the investigation of several target species. In this document, we will review the two main solutions that are being investigated to deliver fixed target collisions to ALICE and we will present some physics opportunities offered by the ALICE detectors in a fixed-target mode.

3. Possible fixed-target implementations

Two solutions are being investigated to deliver fixed-target collisions to ALICE: an internal solid target coupled to a bent crystal to deflect the beam halo and an internal gaseous target. The two methods are described, with more details on the internal solid target solution for which additional studies were carried out with respect to [4]. An estimation of the integrated luminosities that could be collected with the ALICE experiment are given and the ALICE detector acceptance, that depends on the target location, is presented.

3.1. Internal solid target coupled to a bent crystal

In this case, the bent crystal is implemented prior of the ALICE cavern, and the solid target close to the ALICE detectors as described in the following.

3.1.1. Bent crystal implementation

When high-energy charged particles enter a crystal with small angles relative to the crystal planes their transverse motion is governed by the crystal potential averaged along the planes $U(x)$. If the particle angles are smaller than the critical channeling angle $\theta_c = (2U_0/pv)^{1/2}$, where p, v are the particle momentum and velocity and U_0 the depth of the planar potential well, they can be captured into the channeling regime [5]. Channeled positive particles move through a crystal oscillating between two neighboring planes. Therefore, all the processes requiring close collisions with the crystal atoms are strongly suppressed. Channeling is also realized in a bent crystal if its bending radius $R > R_c$, where R_c is the critical bending radius [6, 7], therefore high energy channeled particles can be deflected by bent crystals. The channeling process is used in particle accelerators for beam extraction and splitting [8].

Using crystal channeling, the UA9 Collaboration has experimentally demonstrated the feasibility of crystal-assisted collimation in the SPS [9, 10, 11, 12] and later in the LHC [13], for both proton and Pb-ion beams [14]. Standard collimation rely on a two-stage system. The former collimator imparts multiple-scattering deflection to the halo particles trajectories, eventually deflecting them into the latter secondary absorber. Crystal-assisted collimation, instead, relies on a well-oriented bent crystal promptly deflecting the channeled particles into an absorber. The latter process works more efficiently than the former for three reasons: i) the halo particles intercepted by the crystal turn after turn are very well collimated and therefore have a large probability of being channeled, ii) the halo particles not captured in channeling states at the first hit with the crystal, neither disintegrated in a nuclear reaction, continue circulating in the ring and will have other encounters with the crystal with a high probability of being captured in channeling states after one or more revolutions to be finally deflected into the secondary absorber (multi-pass channeling effect [15]), iii) the channeled particles enter the secondary collimator with a large impact parameter and have a low probability of being back-scattered into the vacuum pipe.

A slight modification of the crystal collimation scheme suggests an elegant way of performing fixed-target physics in modern hadron colliders [16]. An internal target located between the crystal and the absorber may produce high-energy interactions that could be investigated with an appropriate experimental apparatus located downstream of the target itself. The particle flux interacting with the internal target can be continuously

fed by channeling with a bent crystal the otherwise unused halo particle. An example of fixed-target scenario around the ALICE experimental device in the LHC is shown in Fig. 1 left. A small bent crystal, of the size of few millimetres and mounted on an appropriate goniometer [17], could be located upstream of the focusing triplet, just before the TCDD absorber, to channel and deflect the halo particles of LHC beam 1 horizontally, as shown in Fig. 1 right. The target could be located in one of the positions marked in orange in Fig. 1 right. A deflection of the beam halo by 250 μrad, 72 m upstream the Interaction Point 2 (IP2), would allow placing the target at a safe distance of 8 mm from the beam center. The non-interacting particles could be disposed of in an absorber located between the Zero-Degree-Calorimeter (ZDC) and the focusing triplet. The deflected particles follow the green trajectory in Fig. 1 right. The interacting beam halo particles will produce particles into the ALICE detectors, whilst the non-interacting particles will continue their path up to the absorber where they should be completely absorbed.

Important issues not yet investigated concern two aspects: i) the machine protection and ii) the compatibility of the fixed-target operation with the collimation operation. Dedicated studies should be launched in due time. In the discussed configuration, the order of magnitude of the flux of particles on target could be estimated as one third of the circulating intensity more or less evenly distributed over the average run duration.

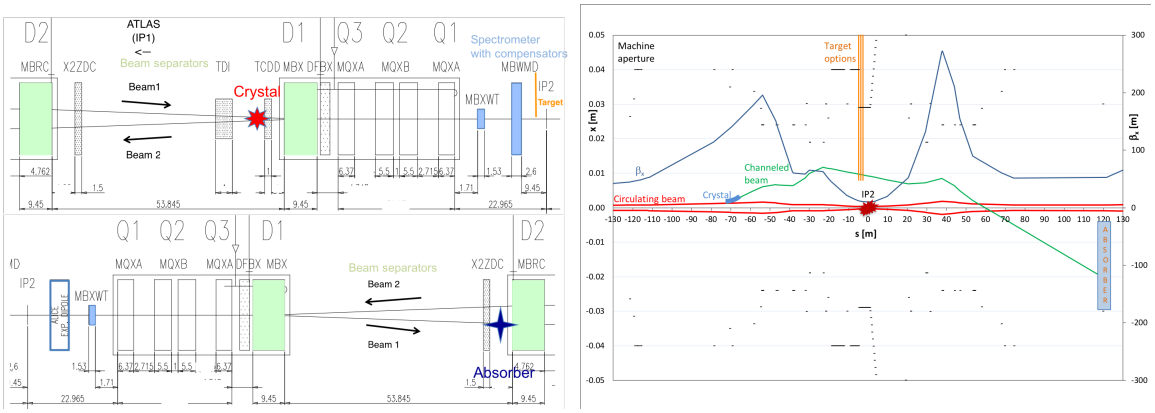

Figure 1: Left: A possible layout for an internal fixed-target experiment at the LHC: a bent crystal is used to deflect the beam halo onto an internal solid target. Right: Particle trajectories for an internal fixed-target experiment: a bent crystal splits and deflects the halo (green) from the circulating beam (red), and sends it on an internal target (orange) placed in front of the ALICE detectors; the non-interacting channeled particles are caught by an absorber downstream; a safe distance is maintained between the channeled beam (green) and the machine aperture (black).

3.1.2. Solid target setup

Several materials are under investigation for the target with low, medium and high atomic mass number. Other constraints shall guide the material for the target itself as well as for the target holder and any other piece close to the interaction between the deflected halo and the target. Among the tight constraints are the compatibility with the vacuum and large melting point. The excess heat must be drained off the target and its holder, in designing dedicated geometry. Light material could be Be (though its toxicity during machining), Ca or C. For heavy materials, Os, Ir or W are good candidates. In-between, materials such as Ti, Ni or Cu could be used. Each target shall be manufactured in an oblong shape, with a radius of 2.5 mm and a total length of 17.5 mm. This design enables a large contact surface between the target and its holder to dissipate the heat. The efficient part of the target is the final round shape, with a thickness that may vary from 0.2 mm to 5 mm. The target holder is designed for maintaining the target between its two sides like a press. This contact holding provides the advantage of a sufficient surface between the target and the holder for heat removal. The top of the holder is connected to the rod of the actuator. Located in a new dedicated tapping, each actuator must be a single-effect pneumatic actuator with a parking position out of the pipe and a position of work inside

the pipe when activated by pressurised air. An electro-valve distributor controls the position of each actuator through a plastic hose and thus is away of the setup. This is to reduce shadow to existing detectors. When the distributor delivers pressurised air to an actuator, it moves on, and when the distributor stops delivering pressure, a spring inside the actuator puts the rod (and so the holder and the target) back in the nominal position. This design provides also a safety position in case of power breakdown. The interface between the inner part of the pipe (vacuum) and the outer environment needs a fine study (mechanical feedthrough). Each tapping receives the target, its holder and the moving parts of the actuator (rod and shock absorber). The static part of the actuator (body) is out of the vacuum. Figure 2 left depicts this setup. It is possible to design a setup with more than one target system, allowing one to have several target types. The target system dimension is 170x50x50 mm. Studies on the target system integration in the experiment are ongoing.

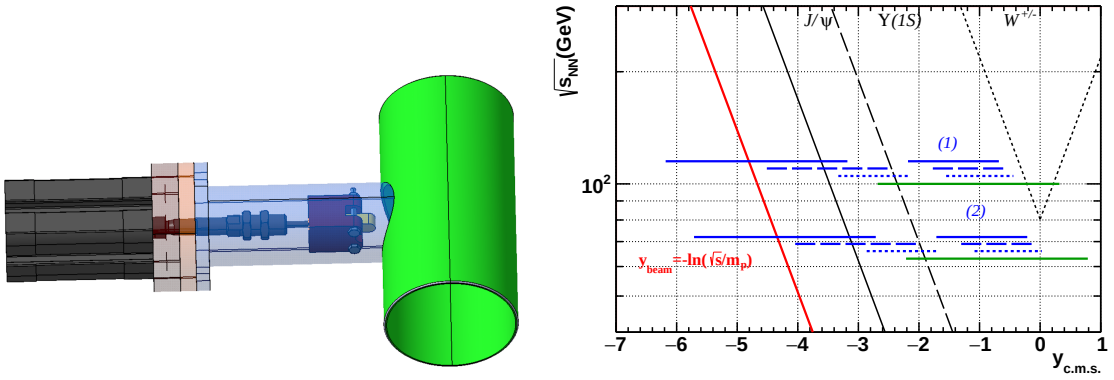

Figure 2: Left: Setup for an internal solid target with one target system. On the right side the pipe section is shown in green. Leftwards are visible the target (yellow), the target holder (brown), the actuator (black) and flanges (pink and orange) with a gasket inside. In translucent blue is the tapping of the pipe. Right: Center-of-mass-rapidity coverage as a function of the colliding energies per nucleon pair. The acceptances of the TPC with reduced track length and Muon Spectrometer of ALICE are represented by the blue lines. The full, long-dashed and short-dashed lines correspond to targets located at the IP, upstream of the IP by $z_{\text{target}} = 2.75$ and 4.7 m, respectively. For comparison, the green lines represent the acceptance of the LHCb detector with a target at the IP. The long-dashed and short-dashed blue lines and the green lines are shifted in energy for a better visibility.

3.2. Internal gas target

An internal gas target such as an atomic beam source system with or without a storage cell could be placed in front of the ALICE detectors. In [4], details are given on the technologies and the achievable instantaneous luminosities for the two following gas target systems: the gas-jet system (as the luminometer of the RHIC) and an atomic beam gas coupled to a storage cell internal to the beam pipe (as the HERMES target at DESY). In both cases, the gas injected can be polarised (H, D and ^{3}He) or unpolarised (H_2, Ne, Ar, Kr, Xe). It requires large space to be installed (most likely outside of the ALICE barrel magnet 7 m away from the nominal IP). A simple unpolarised storage cell without an atomic beam source might potentially be used closer to the nominal IP. In that case, the gas is injected via capillary in the target vacuum chamber.

3.3. Expected luminosities

Table 1 summarises the expected luminosities in ALICE for the solid target coupled to a bent crystal and the gas-jet target. For the bent crystal solution, fluxes of 5×10^8 s^{-1} and 10^5 s^{-1} for proton and lead beams respectively, were considered. For unpolarised gases, the achievable luminosities is limited by the ALICE data taking rate capabilities. Since the data taking rate is mostly driven by the detector occupancy, the given rates could be enhanced by a factor of 10 in *pp* collisions [4].

		ALICE					
		proton beam ($\sqrt{s_{\rm NN}}$= 115 GeV)			Pb beam ($\sqrt{s_{\rm NN}}$= 72 GeV)		
Target		$\mathcal{L}$ [cm^{-2} s^{-1}]	Inel. rate [kHz]	$\int \mathcal{L}$	$\mathcal{L}$ [cm^{-2} s^{-1}]	Inel. rate [kHz]	$\int \mathcal{L}$
Internal gas target (gas-jet option)	$H^{\uparrow}$	4.3×10^{30}	168	43 pb^{-1}	5.6×10^{26}	1	0.56 nb^{-1}
	H_2	2.6×10^{31}	1000	0.26 fb^{-1}	2.8×10^{28}	50	28 nb^{-1}
	$D^{\uparrow}$	4.3×10^{30}	309	43 pb^{-1}	5.6×10^{26}	1.2	0.56 nb^{-1}
	$^3He^{\uparrow}$	8.5×10^{30}	1000	85 pb^{-1}	2.0×10^{28}	50	20 nb^{-1}
	Xe	7.7×10^{29}	1000	7.7 pb^{-1}	8.1×10^{27}	50	8.1 nb^{-1}
Beam splitting	C	3.7×10^{30}	1000	37 pb^{-1}	5.6×10^{27}	18	5.6 nb^{-1}
	Ti	1.4×10^{30}	1000	14 pb^{-1}	2.8×10^{27}	13	2.8 nb^{-1}
	W	5.9×10^{29}	1000	5.9 pb^{-1}	3.1×10^{27}	21	3.1 nb^{-1}

Table 1: Summary table of the achievable integrated luminosities with the ALICE detector accounting for the data-taking-rate capabilities in the collider mode. The solid target lengths are 658 μm (5 mm) for C, 515 μm (5 mm) for Ti, 184 μm (5 mm) for W, with the proton (lead) beam respectively.

3.4. ALICE detectors and acceptances

The detectors of ALICE [18, 19] are optimised for studying the QCD matter created in high-energy collisions of lead nuclei. They are able to cope with high-multiplicity events and to track charged particles down to $p_{\rm T} \sim 0.15$ GeV/c at mid-rapidity. The ALICE CB detectors are embedded into the L3 solenoid magnet that provides a field of 0.5 T parallel to the beam line. In particular, the Time Projection Chamber (TPC) provides track reconstruction as well as particle identification (PID) via the measurement of the specific ionisation energy loss $\mathrm{d}E/\mathrm{d}x$ in the gas volume. The phase space covered by the TPC in pseudorapidity is $|\eta| < 0.9$. The TPC acceptance can be extended by considering only 1/3 of the full radial track length at the cost of worsening the momentum resolution. In that case, the pseudorapidity acceptance is $|\eta| < 1.5$. The Time Of Flight (TOF) detector, with a pseudorapidity coverage of $|\eta| < 0.9$, extends the PID via the measurement of the flight time of the charged particles from the IP. For that purpose the T0 detector located along the beam line measures the event collision time. At forward rapidity, the ALICE MS covers the pseudorapidity range $2.5 < \eta < 4$ in the laboratory frame. It includes a dipole magnet with an integrated field of 3 T·m, five tracking stations, two trigger stations and a system of absorbers. The ALICE upgrade is scheduled for the LS2. Many detectors or their electronics will be upgraded in order to allow for a continuous readout at an interaction rate of 50 kHz in PbPb collisions at $\sqrt{s_{\rm NN}}$ = 5.5 TeV. In pp and pA collisions, a rate of 200 kHz and possibly up to 1 MHz will be possible. The center-of-mass rapidity coverage of the ALICE CB and the MS are shown in blue in Fig. 2 for the two energies accessible with the proton and lead beams, where one assumes massless particles. Three options are used for the target position: located at the IP (full line), upstream of the IP by 2.75 m (dashed line) and 4.7 m (dotted line). The LHCb detector acceptances when the target is located at the nominal IP are also shown for comparison. While the ALICE MS covers a rapidity region close to mid-rapidity ($y_{\rm cms} < 0$), the ALICE CB has the particularity to probe the target rapidity region and the end of the phase space. The MS is suitable to study muon probes close to mid-rapidity and the CB detectors to identify particles at very backward rapidity. In case of a displaced vertex from the nominal IP, studies will be performed to evaluate the material budget and the tracking performances as well as the need of additional detectors for vertexing.

4. Physics opportunities

4.1. Quarkonia

A fixed-target experiment at the centre-of-mass energy of $\sqrt{s_{\rm NN}}$ = 72 GeV provides a complementary coverage to the experiments at (nominal) RHIC and SPS energies, in the region of the QCD matter phase diagram where a formation of the Quark-Gluon Plasma (QGP) is expected. Looking at quarkonium suppression as a function of rapidity and system size would allow one to search for the onset of the QGP formation, and to determine the in-medium modification of the QCD forces. In particular, studies of the suppression of different charmonium and bottomonium states, so called sequential quarkonium melting, provide more insight into the thermodynamic properties of the deconfined matter. Quarkonia are expected to be abundantly produced covering an important region in the $(x, m_{\rm T})$ plane, as shown in Fig. 3 left. Very large yields are expected for charmonia (up to $\sim$ 10^6 J/ψ) in the ALICE MS both in pp and PbA collisions[2] considering one LHC year of data taking. The Υ(1S) will also be within reach. At this centre-of-mass energy the recombination effect for charmonia is predicted to be negligible. Thanks to the excellent capabilities of ALICE to operate in a high multiplicity environment, quarkonium measurements in central AA collisions would be unique to ALICE with respect to LHCb, at forward $y_{\rm lab}$. Moreover, precise measurements in pA collisions will allow to determine the modification of the quarkonium production due to the cold nuclear matter effects. In pA collisions, Υ(1S) could be used to probe large x-gluon distribution, which is the least known nPDF [20], in the target ($0.1 < x < 1$) in order to constrain anti-shadowing and EMC effects.

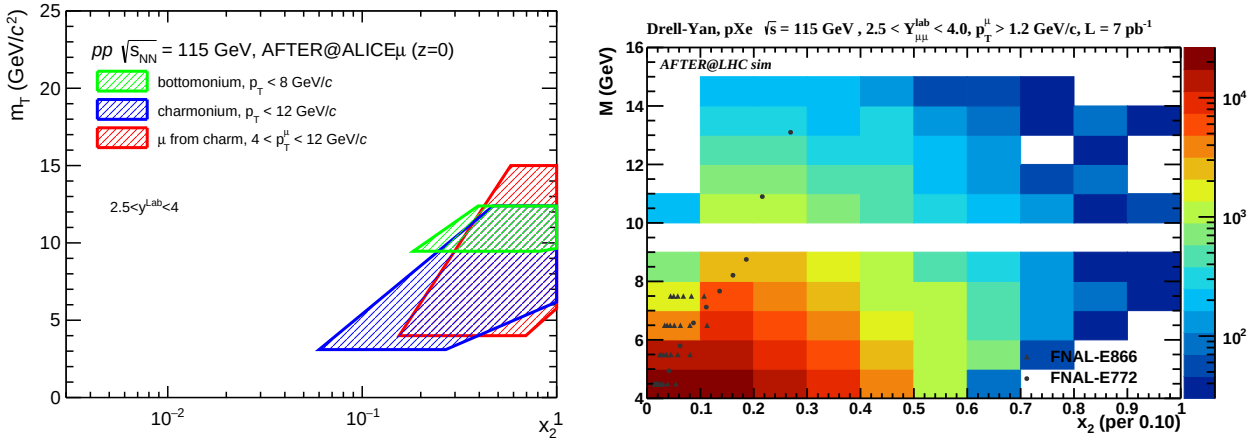

Figure 3: Left: Typical kinematical reach in x_2 and the scale (chosen to be $m_{\rm T}$) of the fixed-target mode with a detector acceptance like ALICE. Right: Kinematical reach for Drell-Yan lepton-pair production with an ALICE-like detector in pXe collisions at $\sqrt{s}$ = 115 GeV with an acceptance of $2.5 < \eta_\mu^{\rm lab} < 4$ and $p_{\rm T}^\mu > 1.2$ GeV. Colours correspond to expected yields of the Drell-Yan signal in each kinematical region, and each coloured cell contains at least 30 events.

4.2. Open Heavy Flavours

A complete set of heavy flavour (HF) studies performed in fixed-target mode from elementary collisions to most complex heavy nuclei collisions can widely increase our understanding of the nucleon and nuclear structure at large-x as well as our understanding of the hot nuclear matter created in heavy-ion collisions. Indeed, a non-perturbative intrinsic contribution to the heavy quark PDF in the proton is expected from QCD diagrams in which the heavy quark pair is attached by two or more gluons to the valence quarks. A non-perturbative intrinsic charm component in the proton would modify the inclusive D meson yield, especially at large transverse momentum or very backward rapidities. A good knowledge of charmed meson production

[2]The largest atomic mass number considered in this document is W for the solid target and Xe for the gas target.

is important in high energy cosmic ray observations since it will reduce the uncertainty on the prompt atmospheric neutrino flux. Figure 4 left shows the rapidity-differential cross section of D^0 mesons in the lab for pH_2 collisions at $\sqrt{s}$ = 72 GeV, as well as the expected yield per year per 0.1 y_{lab} unit. At $y_{lab} \sim 1$, about 3000 D^0 are expected to be produced per 0.1 rapidity unit per year. The ALICE CB in fixed-target mode is well suited to study the large-x intrinsic charm component in the proton, since it probes the end of the D meson phase space, at very backward rapidity, as illustrated with the black lines of Fig. 4 left, for three different target locations. In proton-nucleus collisions, HF production can be used to constrain the high-x nuclear gluon distribution, which is the least known nPDF (see [20] at LHC energies). Finally, in AA collisions, open HF are sensitive to the dynamics of the formed medium and could be used to determine the fundamental properties of the QGP, such as the transport coefficients and the charm quark diffusion coefficients. Measurements of open HF suppression at large rapidities and high p_T can help discrimate between models of the heavy quark interactions with the QGP (radiative versus collisional energy loss). In Fig. 4 right, the rapidity-differential cross section of D^0 mesons in the lab for PbW collisions at $\sqrt{s_{NN}}$ = 72 GeV, as well as the expected yield per year per 0.1 y_{lab} unit, is shown. In the backward rapidity region covered by the ALICE CB, at $y_{lab} \sim 1$ about 100 D^0 are expected to be produced per 0.1 rapidity unit per year. Note that all the HF measurements proposed in the ALICE CB would be performed in a rapidity domain only accessible by the ALICE detector.

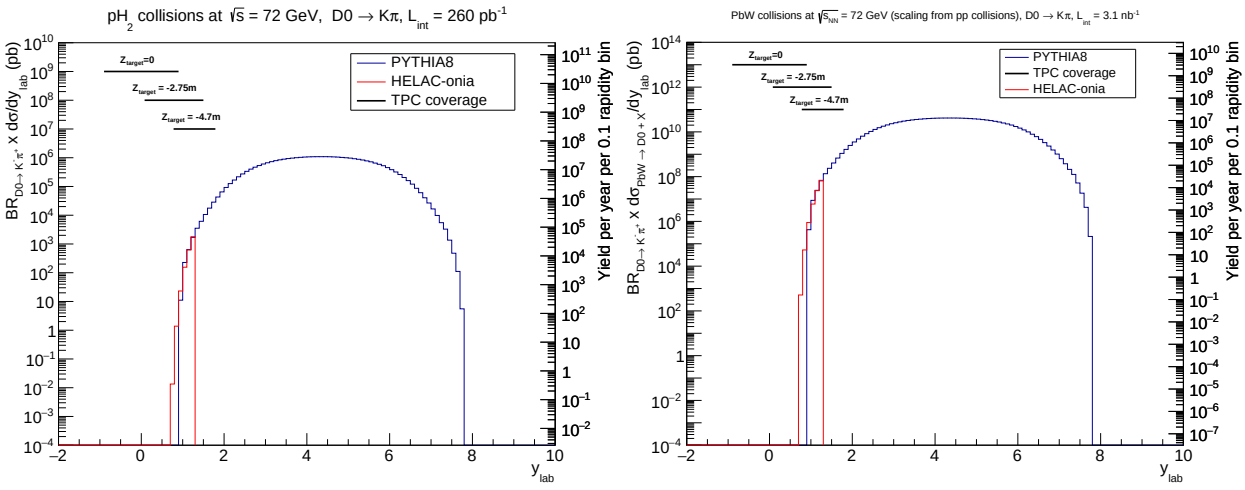

Figure 4: The rapidity-differential cross section of D^0 mesons (measured via the Kπ decay channel) in the lab for pH_2 collisions at $\sqrt{s}$ = 72 GeV (left) and PbW collisions at $\sqrt{s_{NN}}$ = 72 GeV (right), as well as the expected yield per year per 0.1 y_{lab} unit. Simulations were performed with PYTHIA8 [21] (blue histogram). The shape of the rapidity distribution at the end of phase space was also studied with the HELAC-onia [22] MC generator (red histogram).The PbW spectra are obtained by scaling the pH_2 spectra by the number of nucleons, assuming no medium effects. The ALICE TPC coverage is indicated with black lines for three different target locations.

4.3. Drell-Yan

Currently, initial-state effects in pA collisions are extrapolated to AA collisions assuming a linear factorisation of these effects. This assumption can be tested using electromagnetic probes, such as the Drell-Yan process. It is important to perform the studies in a broad x range where the variation of the nuclear modifications in pA collisions are expected to be significant. Figure 3 right shows the kinematic reach for the Drell-Yan production with an ALICE-like detector. A precise measurement of the Drell-Yan pair production with the ALICE MS can probe initial state effects on quarks of momentum fraction $0.05 < x < 0.8$ at a mass scale of $M_{\mu\mu} > 4$ GeV/c^2 from pA to AA collisions. A systematic investigation of Drell-Yan production in all systems including access to central AA collisions would only be possible in ALICE. The correlated background from $b\bar{b}$ and $c\bar{c}$ pairs in the dimuon decay channel, that is a challenge in collider experiments, is

largely reduced at the lower centre-of-mass energy of the fixed-target mode and at backward rapidity, with respect to the TeV energy range. Precise high-x nuclear Drell-Yan data would provide a unique access to the sea quarks and combined with the gluon EMC and its nuclear number dependence, would shed light on the origin of the EMC effect.

4.4. Antiproton

Measurements of antiproton production cross sections in pH and pA collisions[3] are important inputs for theoretical calculations of the secondary[4] cosmic antiproton spectrum [23, 24, 25]. The measurement of a cosmic antiproton excess with respect to expectations from secondary antiproton production would open new perspectives on the indirect detection of dark matter or unknown astrophysical mechanisms of cosmic ray acceleration. Complementarily to LHCb [26], the ALICE CB can measure very slow antiprotons down to few hundred MeV momentum. Measuring slow antiprotons produced with the LHC proton beam on a nuclear target is equivalent to the case where the nuclear target travels at TeV energies, hit an interstellar proton at rest and produces an antiproton with high energy. Figure 5 shows the rapidity-differential (left) and energy-differential (right) antiproton cross section in $p\mathrm{H}_2$ collisions at $\sqrt{s} = 115$ GeV. Thanks to the large antiproton yields expected in $p\mathrm{H}_2$ collisions (larger than 10^8 per 0.1 rapidity unit per year), the ALICE CB is well placed to help constraining the uncertainty on the antiproton spectrum.

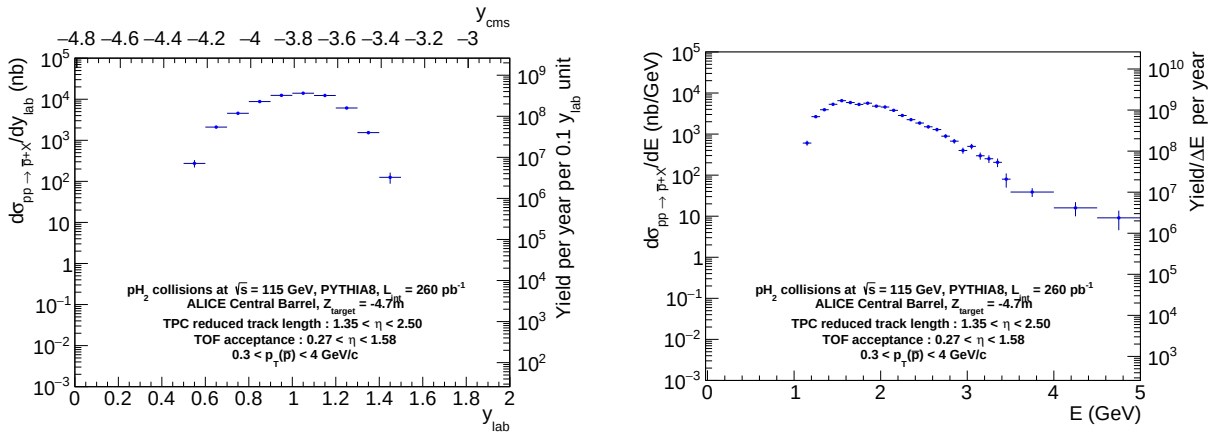

Figure 5: Rapidity-differential (left) and energy-differential (right) antiproton cross section in $p\mathrm{H}_2$ collisions at $\sqrt{s} = 115$ GeV. The ALICE CB acceptance is considered, assuming a target located at $z = -4.7$ m. On the vertical axis is also shown the antiproton yield per year per 0.1 $\mathrm{y_{lab}}$ unit (left), per ΔE (right).

4.5. Identified charged particles

Measurements of identified particles up to very large rapidities would complement the limiting fragmentation studies carried out by the BRAHMS and PHOBOS experiments at RHIC. In addition, particle yields and flow coefficients measured at large rapidities are powerful tools to constrain the temperature dependence of the medium shear viscosity [27]. Thermal model calculations also indicate that the temperature and baryonic chemical potential depend on the rapidity [28, 29, 30] suggesting that one can perform a rapidity scan of the QGP phase diagram in a complementary approach to the Beam Energy Scan programme of RHIC. In few hours of PbA data taking, it would be already possible to collect up to 10^6 minimum bias events with the ALICE CB which would allow one to reach an absolute statistical uncertainty of 0.01 on the elliptic flow

[3] He, C, N, O

[4] Secondary antiproton originate from the high energy scattering between the interstellar matter and primary cosmic rays.

coefficient v_2 for pions and protons, 0.02 for kaons, and 0.05 for antiprotons in semi-central events[5] (see Fig. 6 left).

4.6. Strangeness

Distributions of longitudinally polarised (anti)quarks inside the nucleon are still poorly known, especially the distribution of polarised strange and antistrange quarks (and their possible asymmetry). On top of being a key information on the structure of matter, they also enter in theoretical calculations for astrophysics (modeling of core-collapse supernova explosions). Since both the quark structure and the total spin of the nucleon arise from the valence quark PDFs at high x, it is therefore crucial to collect precise data in this kinematic range. Thanks to the large yields[6] ($\sim 10^8$ per 0.1 rapidity unit per year at $y_{\rm lab} \sim 1$) of Λ expected to be produced in the ALICE CB by using a longitudinally polarised target with the proton beam, a precise measurement (with sub-percent precision, see figure 6 right) of the longitudinal spin transfer D_{LL} of the Λ hyperon could be carried out. So far only limited experimental results exist with poor precision[31, 32, 33]. The excellent particle identification capabilities of the ALICE CB would give a unique opportunity to study the spin-dependent strange quark (antiquark) densities at bakward rapidity, at large x in the target ($0.35 < x < 0.7$).

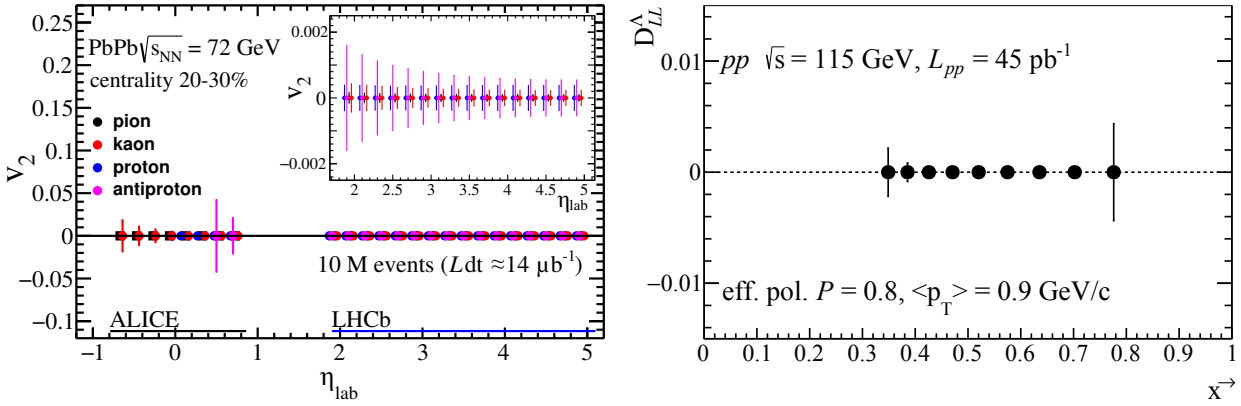

Figure 6: Left: Projections of the statistical uncertainty on the measurement of the elliptic flow of identified hadrons (with $p_T > 0.2$ GeV/c for the ALICE CB) as a function of η_{lab}, in PbA collisions at $\sqrt{s_{\rm NN}} = 72$ GeV, from EPOS [34] simulations. Right: The statistical precision expected for the longitudinal spin transfer D_{LL} to Λ hyperons with the ALICE CB and a target located at $z = -4.7$ m, as a function of x. The Λ yields are calculated using PYTHIA8, taking into account the acceptance of the ALICE TPC and TOF detectors and a realistic reconstruction efficiency of Λ baryons in the ALICE experiment [35].

4.7. Charmonium and pentaquark photoproduction

Exclusive J/ψ photoproduction is known to be sensitive to gluon Generalised Parton Distributions (GPD) at leading order [36]. ALICE in fixed-target mode would have a unique opportunity to study the yet unknown GPD E_g thanks to the measurement of Single Transverse Spin Asymmetries of photoproduced J/ψ in $p\mathrm{H}^{\uparrow}$ collisions [37, 38]. About 200 photoproduced J/ψ per year[5] are expected to be produced in the ALICE MS acceptance in $p\mathrm{H}^{\uparrow}$ collisions, as can be seen in Fig. 7 which shows the rapidity-differential cross section of the photoproduced J/ψ in the dimuon decay channel as well as the yield per year per 0.1 $y_{\rm lab}$ unit. Moreover, the photoproduction of hidden charm pentaquark states might be possible in the ALICE CB acceptance which allows for the access to low photon-proton centre-of-mass energies ($W_{\gamma p} \sim 5$ GeV). Figure 7 right shows the rapidity-differential cross section of the photoproduced J/ψ, in $p\mathrm{H}_2$ collisions in the dielectron decay channel

[5]These studies were performed assuming a vertex position at the ALICE IP.
[6]These studies were performed assuming a vertex position at 4.7 m from the ALICE IP.

as well as the yield per year per 0.1 y_{lab} unit. From the J/ψ photoproduction yield, it is possible to estimate the number of photoproduced pentaquarks, based on the signal over background ratio given in [39]. About 2 to 20 pentaquarks[5] are expected to be produced in the ALICE CB (in an acceptance region not covered by LHCb) per year in $p\mathrm{H}_2$ collisions.

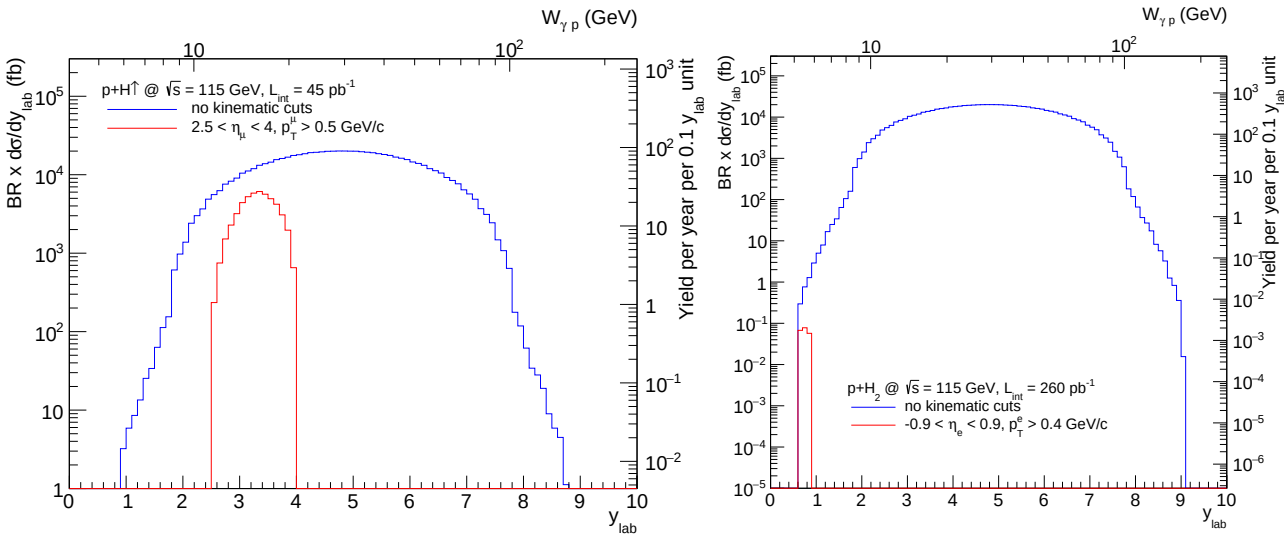

Figure 7: Rapidity-differential cross section of the photoproduced J/ψ in the dimuon decay channel (left) and dielectron decay channel (right), as well as the yield per year per 0.1 y_{lab} unit, in $p\mathrm{H}^{\uparrow}$ collisions (left) and $p\mathrm{H}_2$ collisions (right) at $\sqrt{s}$ = 115 GeV. The blue histogram is obtained from STARLIGHT[40] simulations without applying kinematical cut, while the red histogram is obtained after applying ALICE acceptance cuts.

4.8. Other opportunities

Investigations are ongoing to extend the ALICE rapidity coverage for several observables thanks to combined measurements of muons detected both in the ALICE CB and MS [41].

5. Conclusion

A fixed-target programme in ALICE offers extraordinary opportunities in the area of high-energy nuclear and particle physics. Heavy-flavor and Drell-Yan productions in pp and pA collisions will allow one to probe the high-x content of the nucleon and nuclei. Especially, the ALICE central barrel will give unique access to the very high-x ($x \to 1$) structure of nucleon and nuclei. The mentioned probes as well as the identified charged particles will provide constraints on the Quark Gluon Plasma properties when using the lead beam on nuclear target. Antiproton measurements in specific kinematic ranges are also important inputs to astroparticle physics in pA collisions. In addition, installation of a polarised target will open the door to a new area of research at the LHC. This physics programme could benefit from a significant data taking time in ALICE, in particular with the proton beam. Dedicated studies will be needed to address the possible limitations of the proposed technical implementations (beam halo extraction by using a bent crystal or gas target) and the compatibility with the LHC operation. Studies are ongoing on the technical feasibility of the target system integration in the experiment, as well as simulation studies to evaluate the ALICE apparatus tracking performances for a displaced vertex from the nominal interaction point. These studies will benefit from the Horizon 2020 grant *STRONG-2020*. An installation could be foreseen during the Long Shutdown 3.

6. References

[1] A. B. Kurepin, N. S. Topilskaya, and M. B. Golubeva, "Charmonium production in fixed-target experiments with SPS and LHC beams at CERN," *Phys. Atom. Nucl.* **74** (2011) 446–452. [Yad. Fiz.74,467(2011)].

[2] S. J. Brodsky, F. Fleuret, C. Hadjidakis, and J. P. Lansberg, "Physics Opportunities of a Fixed-Target Experiment using the LHC Beams," *Phys. Rept.* **522** (2013) 239–255, arXiv:1202.6585 [hep-ph].

[3] J. P. Lansberg, G. Cavoto, C. Hadjidakis, J. He, C. Lorcé, and B. Trzeciak, "Physics at a Fixed-Target Experiment Using the LHC Beams,," *Adv. High. Energy Phys.* **2015** (2015) 2.

[4] C. Hadjidakis *et al.*, "A Fixed-Target Programme at the LHC: Physics Case and Projected Performances for Heavy-Ion, Hadron, Spin and Astroparticle Studies," arXiv:1807.00603 [hep-ex].

[5] J. Linhard *K. Dan. Vidensk. Selsk. Mat. Fys. Medd.34* **14** (1965) .

[6] D. Gemmell *Rev.Mod.Physics* **46** (1974) 129.

[7] E. Tsyganov *Preprint TM-682, TM-684, Fermilab, Batavia* .

[8] V. Biryukov *et al.*, "Crystal channeling and its application at high-energy accelerators," *Springer-Verlag, Berlin* (1997) .

[9] W. Scandale *et al.*, "First results on the SPS beam collimation with bent crystals," *Phys. Lett.* **B692** (2010) 78–82.

[10] W. Scandale *et al.*, "Strong reduction of the off-momentum halo in crystal assisted collimation of the SPS beam," *Phys. Lett.* **B714** (2012) 231–236.

[11] W. Scandale *et al.*, "Optimization of the crystal assisted collimation of the SPS beam," *Phys. Lett.* **B726** (2013) 182–186.

[12] W. Scandale *et al.*, "Observation of strong leakage reduction in crystal assisted collimation of the SPS beam," *Phys. Lett.* **B748** (2015) 451–454. [Erratum: Phys. Lett.B750,666(2015)].

[13] W. Scandale *et al.*, "Observation of channeling for 6500 GeV/ c protons in the crystal assisted collimation setup for LHC," *Phys. Lett.* **B758** (2016) 129–133.

[14] W. Scandale *et al.*, "Comparative results on collimation of the SPS beam of protons and Pb ions with bent crystals," *Phys. Lett.* **B703** (2011) 547–551.

[15] X. Altuna *et al.*, "High efficiency multipass proton beam extraction with a bent crystal at the SPS," *Phys. Lett.* **B357** (1995) 671–677.

[16] **UA9** Collaboration, L. Burmistrov, G. Calderini, Y. Ivanov, L. Massacrier, P. Robbe, W. Scandale, and A. Stocchi, "Measurement of Short Living Baryon Magnetic Moment using Bent Crystals at SPS and LHC," Tech. Rep. CERN-SPSC-2016-030. SPSC-EOI-012, CERN, Geneva, Jun, 2016. https://cds.cern.ch/record/2194564.

[17] M. Butcher, A. Giustiniani, R. Losito, and A. Masi tech. rep.

[18] **ALICE** Collaboration, K. Aamodt *et al.*, "The ALICE experiment at the CERN LHC," *JINST* **3** (2008) S08002.

[19] **ALICE** Collaboration, B. B. Abelev *et al.*, "Performance of the ALICE Experiment at the CERN LHC," *Int. J. Mod. Phys.* **A29** (2014) 1430044, arXiv:1402.4476 [nucl-ex].

[20] A. Kusina, J.-P. Lansberg, I. Schienbein, and H.-S. Shao, "Gluon Shadowing in Heavy-Flavor Production at the LHC," *Phys. Rev. Lett.* **121** no. 5, (2018) 052004, arXiv:1712.07024 [hep-ph].

[21] T. Sjostrand, S. Mrenna, and P. Z. Skands, "A Brief Introduction to PYTHIA 8.1" *Comput. Phys. Commun.* **178** (2008) 852–867, arXiv:0710.3820 [hep-ph].

[22] H.-S. Shao, "HELAC-Onia: An automatic matrix element generator for heavy quarkonium physics," *Comput. Phys. Commun.* **184** (2013) 2562–2570, arXiv:1212.5293 [hep-ph].

[23] I. V. Moskalenko and A. W. Strong, "Production and propagation of cosmic ray positrons and electrons," *Astrophys. J.* **493** (1998) 694–707, arXiv:astro-ph/9710124 [astro-ph].

[24] A. E. Vladimirov, S. W. Digel, G. Johannesson, P. F. Michelson, I. V. Moskalenko, P. L. Nolan, E. Orlando, T. A. Porter, and A. W. Strong, "GALPROP WebRun: an internet-based service for calculating galactic cosmic ray propagation and associated photon emissions," *Comput. Phys. Commun.* **182** (2011) 1156–1161, arXiv:1008.3642 [astro-ph.HE].

[25] E. Orlando, G. Johannesson, I. V. Moskalenko, T. A. Porter, and A. Strong, "GALPROP cosmic-ray propagation code: recent results and updates," 2017. arXiv:1712.09755 [astro-ph.HE]. http://inspirehep.net/record/1645188/files/arXiv:1712.09755.pdf.

[26] **LHCb** Collaboration, R. Aaij *et al.*, "Measurement of antiproton production in pHe collisions at $\sqrt{s_{NN}}$ = 110 GeV," *Submitted to: Phys. Rev. Lett.* (2018) , arXiv:1808.06127 [hep-ex].

[27] G. Denicol, A. Monnai, and B. Schenke, "Moving forward to constrain the shear viscosity of QCD matter," *Phys. Rev. Lett.* **116** no. 21, (2016) 212301, arXiv:1512.01538 [nucl-th].

[28] F. Becattini and J. Cleymans, "Chemical Equilibrium in Heavy Ion Collisions: Rapidity Dependence," *J. Phys.* **G34** (2007) S959–964, arXiv:hep-ph/0701029 [hep-ph].

[29] I. Karpenko, "Rapidity scan in heavy ion collisions at $\sqrt{s_{\rm NN}}$ = 72 GeV using a viscous hydro + cascade model," arXiv:1805.11998 [nucl-th].

[30] V. Begun, D. Kikola, V. Vovchenko, and D. Wielanek, "Estimation of the freeze-out parameters reachable in the AFTER@LHC project," arXiv:1806.01303 [nucl-th].

[31] **STAR** Collaboration, B. I. Abelev *et al.*, "Longitudinal Spin Transfer to Lambda and anti-Lambda Hyperons in Polarized Proton-Proton Collisions at $\sqrt{s}$ = 200 GeV," *Phys. Rev.* **D80** (2009) 111102, arXiv:0910.1428.

[32] **STAR** Collaboration, J. Adam *et al.*, "Improved measurement of the longitudinal spin transfer to Λ and $\bar{\Lambda}$ hyperons in polarized proton-proton collisions at $\sqrt{s}$ = 200 GeV," arXiv:1808.07634 [hep-ex].

[33] **COMPASS** Collaboration, M. Alekseev *et al.*, "Measurement of the Longitudinal Spin Transfer to Lambda and Anti-Lambda Hyperons in Polarised Muon DIS," *Eur. Phys. J.* **C64** (2009) 171–179, arXiv:0907.0388 [hep-ex].

[34] T. Pierog, I. Karpenko, J. M. Katzy, E. Yatsenko, and K. Werner, "EPOS LHC: Test of collective hadronization with data measured at the CERN Large Hadron Collider," *Phys. Rev.* **C92** no. 3, (2015) 034906, arXiv:1306.0121 [hep-ph].

[35] **ALICE** Collaboration, K. Aamodt *et al.*, "Strange particle production in proton-proton collisions at sqrt(s) = 0.9 TeV with ALICE at the LHC," *Eur. Phys. J.* **C71** (2011) 1594, arXiv:1012.3257 [hep-ex].

[36] D. Yu. Ivanov, A. Schafer, L. Szymanowski, and G. Krasnikov, "Exclusive photoproduction of a heavy vector meson in QCD," *Eur. Phys. J.* **C34** no. 3, (2004) 297–316, arXiv:hep-ph/0401131 [hep-ph]. [Erratum: Eur. Phys. J.C75,no.2,75(2015)].

[37] L. Massacrier, J. P. Lansberg, L. Szymanowski, and J. Wagner, "Quarkonium-photoproduction prospects at a fixed-target experiment at the LHC (AFTER@LHC)," in *Photon 2017: International Conference on the Structure and the Interactions of the Photon and 22th International Workshop on Photon-Photon Collisions and the International Workshop on High Energy Photon Colliders CERN, Geneva, Switzerland, May 22-26, 2017*. 2017. arXiv:1709.09044 [nucl-ex]. http://inspirehep.net/record/1625748/files/arXiv:1709.09044.pdf.

[38] J. Koempel, P. Kroll, A. Metz, and J. Zhou, "Exclusive production of quarkonia as a probe of the GPD E for gluons," *Phys. Rev.* **D85** (2012) 051502, arXiv:1112.1334 [hep-ph].

[39] Q. Wang, X.-H. Liu, and Q. Zhao, "Photoproduction of hidden charm pentaquark states $P_c^+(4380)$ and $P_c^+(4450)$," *Phys. Rev.* **D92** (2015) 034022, arXiv:1508.00339 [hep-ph].

[40] S. R. Klein, J. Nystrand, J. Seger, Y. Gorbunov, and J. Butterworth, "STARlight: A Monte Carlo simulation program for ultra-peripheral collisions of relativistic ions," *Comput. Phys. Commun.* **212** (2017) 258–268, arXiv:1607.03838 [hep-ph].

[41] **ALICE** Collaboration, S. Acharya *et al.*, "Energy dependence of exclusive J/ψ photoproduction off protons in ultra-peripheral p-Pb collisions at $\sqrt{s_{\rm NN}}$ = 5.02 TeV," arXiv:1809.03235 [nucl-ex].